Nanoscale

Binary small molecule organic nanoparticles exhibit both direct and diffusion-limited ultrafast charge transfer with NIR excitation

Journal:	*Nanoscale*
Manuscript ID	NR-ART-11-2018-009619
Article Type:	Paper
Date Submitted by the Author:	28-Nov-2018
Complete List of Authors:	Kudisch, Bryan; Princeton University, Chemistry Maiuri, Margherita; Politecnico di Milano Dipartimento di Chimica Materiali e Ingegneria Chimica Giulio Natta Wang, Leon; Princeton University Department of Chemical and Biological Engineering, Lim, Tristian; Princeton University Department of Chemical and Biological Engineering, Lu, Hoang; Princeton University Department of Chemical and Biological Engineering, Lee, Victoria; Princeton University Department of Chemical and Biological Engineering Prud'homme, Robert; Princeton University, Department of Chemical Engineering Scholes, Gregory; Princeton University, Chemistry

Journal Name

ARTICLE

Binary small molecule organic nanoparticles exhibit both direct and diffusion-limited ultrafast charge transfer with NIR excitation

Received 00th January 20xx,
Accepted 00th January 20xx

DOI: 10.1039/x0xx00000x

www.rsc.org/

Bryan Kudisch[1], Margherita Maiuri[1†], Leon Wang[2], Tristan Lim[2], Hoang Lu[2†], Victoria Lee[2], Robert K. Prud'homme[2], Gregory D. Scholes[1*]

Here we describe a facile, one-step synthesis of a binary organic nanoparticle composed completely of NIR-absorbing small molecules, a quatterylene diimide and a vanadyl napthalocyanine, using Flash Nanoprecipitation. We show that the molecules are co-encapusalted within an amphiphilic block copolymer shell by observing distinct ultrafast dynamics in the binary nanoparticles compared to nanoparticles of their individual components, which we rationalize as a photoinduced charge transfer. We then draw similarities between the charge transfer dynamics studied in our system and the charge dissociation process in macroscale organic bulk heterojunction blends for OPV applications by assigning the ultrafast time component (~10 ps) to directly interfacial charge transfer and the slow component (70-200 ps) to diffusion limited charge transfer. This discovery can inspire mixed-composition nanoparticles with new functionality for optoelectronic and theranostic applications.

Introduction

In an effort to gain insight into the photophysical interactions between organic semiconductors and dyes either in the condensed phase, like in the active layer for organic photovoltaics, or in a solution mixture, like for homogeneous photocatalysis, a relatively new approach is to study them in nanoparticle (NP) form.[1-4] Organic nanoparticles can generally display rich and disparate properties compared to the parent molecules due to electronic interactions between nearby chromophores, akin to their mascroscale properties observed in their thin films[5-8]. However, most reported organic nanoparticles are unitary in composition, meaning that they are composed of only one type of molecule or polymer. Most synthetic methods rely on the "crashing out" of an organic solution of the organic component of interest upon injection into water; hence one would expect these methods to result in a mixture of unitary molecules upon the inclusion of multiple organic components in the organic solution precursor.[9, 10]

The development of multicomponent organic nanoparticles could bring a number of the exotic photophysical properties of organic material blends to the nanoscale.[11, 12] While unitary organic nanoparticles already have functional variability derived from the immense power of organic chemistry, this power is multiplied when one considers the possibility of even just a binary organic nanoparticle, where now each of the individual components can be independently tailored towards optimizing specific intermolecular interactions between identical molecules or between components. Reports of multicomponent organic molecules and their photophysical dynamics are few and far in between, with most reports stemming from the past decade, relying on multistep synthetic procedures, and generally one of their components is polymeric, which may aid in the reprecipitation of small molecules on the polymeric seed nanoparticle or vice-versa.[13-15] Further, of these reports, none have demonstrated appreciable absorption in the near-IR (NIR) region of the absorption spectrum, which is a region of interest for biomedical applications of organic nanoparticles.[16-19]

In this study, we report and investigate the photophysical properties and dynamics of one of the first reported solely small-molecule binary organic nanoparticles. Using Flash Nanoprecipitation, we have synthesized and characterized nanoparticles comprising Lumogen® IR 788, a quaterrylene derivative which will be henceforth referred to as QDI, as well as vanadyl 2,11,20,29-tetra-tert-butyl-2,3-naphthalocyanine which will be henceforth referred to as VONc. Upon photoexcitation in the NIR, we show that the binary nanoparticle undergo both ultrafast and delayed photoinduced charge transfer, providing strong support for

1. *Department of Chemistry, Princeton University, Princeton, NJ 08544, USA*
2. *Department of Chemical and Biological Engineering, Princeton University, Princeton, NJ 08544, USA.*
†Margherita Maiuri, Politecnico di Milano, Milano, MI, Italy, Hoang Lu, Johnson and Johnson, NJ. Electronic Supplementary Information (ESI) available: Tabulated formulations of QDI, VONc, and Binary nanoparticles 1-3. DLS of QDI, VONc, and Binary nanoparticles 1-3. TEM of QDI, VONc, and Binary nanoparticle 2. Absorption and emission spectra of QDI in toluene and VONc in toluene, along with emission spectra of QDI, VONc, and Binary nanoparticle 1. Pump probe spectra and global analysis of QDI and VONc, both in solution and in nanoparticle form, as well as for Binary 1. Late time pump probe spectra of Binary 1 and Binary 3 with different pump excitation is also reported. Pump-probe anisotropy of QDI nanoparticles is also included. See DOI: 10.1039/x0xx00000x

our assertion of OPV-like molecular blends within individual organic nanoparticles.

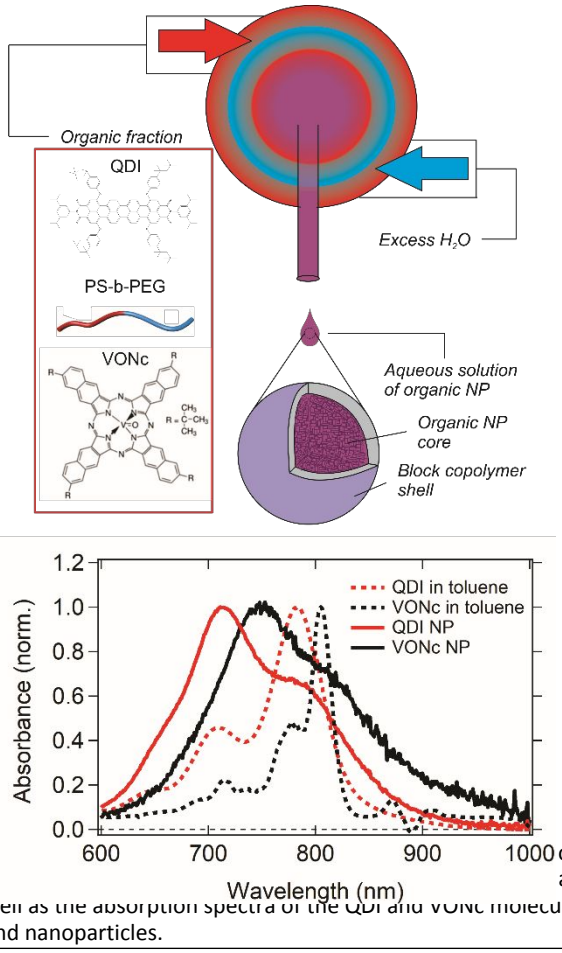

F of u as well as the absorption spectra of the QDI and VONc molecules and nanoparticles.

Experimental Methods

Reagents. QDI (Anthra[9'',1'',2'':6,5,10;10'',5'',6'':6',5',10']dianthra[2,1,9-def:2',1',9'-d'e'f']diisoquinoline1,3,12,14(2H,13H)-tetrone, 2,13-bis[2,6-bis(1-methylethyl)phenyl]-5,10,16,21-tetrakis[4-(1,1,3,3- tetramethylbutyl)phenoxy]) was obtained from BASF SE (Ludwigshafen, Germany) as Lumogen® IR 788. VONc (vanadyl 2,11,20,29-tetra-tert-butyl-2,3-naphthalocyanine) was purchased from Sigma-aldrich. Both chromophores were used as-is without additional purification or modification steps. 1.6 kDa polystyrene blocked with 5.0 kDa polyethylene glycol (PS-b-PEG) was obtained from Polymer Source (Dorval, Canada) and used as nanoparticle stabilizer. The nanoparticle co-core used is 1.9 kDa polystyrene homopolymer (Polymer Source).

Flash NanoPrecipitation. QDI only, VONc only, and all binary nanoparticles were synthesized by using Flash Nanoprecipitation, a scalable and continuous nanoparticle synthesis technique.[20-22] The prementioned organic chromophores and an amphiphilic stabilizer, in our case polystyrene blocked with polyethylene glycol (PS-b-PEG, 5k-1.6k) were dissolved in a water-miscible organic solvent, such as THF or acetone. Through micro-mixing of the organic solution with Milli-Q DI water using a confined impinging jet reactor (CIJ), the organic chromophores precipitate in the aqueous environment and are rapidly stabilized by the amphiphilic block co-polymer. The mixed streams were then diluted 10-fold into an aqueous collecting solvent. Through this process, PS-b-PEG forms micellar-like structures in such a way that essentially corrals the water-insoluble organic molecules into its core, forming a shell of block copolymer around a nanoscale agglomerate of the organic components in the precursor solution. In this way, since nanoparticle formation is driven by competing mixing and precipitation timescales, we hypothesized that the inclusion of a second organic chromophore could create a molecular mixture within individual nanoparticles. Physical characterization by dynamic light scattering (DLS) and transmission electron microscopy (TEM) shows spherical nanoparticles with relatively low polydispersity and average hydrodynamic sizes ranging from 80 to 200 nm depending on molecular and PS-b-PEG concentrations (S1-2). Of particular note is that for all nanoparticles, TEM could not distinguish between the organic molecule core and the block copolymer shell, nor the VONc from the QDI in the binary nanoparticles (S3-5). Further, a representative TEM diffractogram of Binary 1 is shown in figure S5, showing no discernable crystallinity.

Dynamic light scattering (DLS). Nanoparticle size and polydispersity was characterized using dynamic light scattering (Malvern Zetasizer Nano, Malvern Instruments). FNP formulations were diluted 10-fold into Milli-Q DI water and measurements were made using a glass cuvette (3500 uL, Sigma Aldrich). Size distributions are reported as Z-averages from backscatter measurements.

Transmission electron microscopy (TEM). Nanoparticle morphology was investigated using Transmission Electron Microscopy (Philips CM200 FEG). FNP formulations were diluted 100-fold into Milli-Q DI water.10ul of the diluted NP solution was then flash frozen onto a pre-chilled copper grid (Sigma Aldrich) at -80 ℃ and lyophilized for 12 hours. TEM was then conducted on the lyophilized samples at an accelerating voltage of 200 kV.

Steady-state absorption and fluorescence spectroscopy. Steady state absorption spectra were taken with an Agilent Cary 60 Spectrophotometer (Agilent, Santa Clara, CA) using a 2 mm glass cuvette (Starna Cells, Inc, Atascadero, CA), an integration time of 0.1 s, and a step size of 1 nm. For the absorption spectra taken for the analysis of the $VONc^+$ absorption spectra, a 10 mm glass cuvette (Starna Cells, Inc, Atascadero, CA) was used with a Cary 6000i Spectrophotometer (Agilent, Santa Clara, CA) with the same sampling procedures. Steady state fluorescent spectra were taken with the same 10 mm cuvette using a Quantamaster 400 (HORIBA Scientific, Edison, NJ) with excitation wavelength at 710 nm and excitation and emission slits set to 20 nm in the case of nonfluorescent samples, and 10 nm in the case of the QDI in toluene solution. The emission monochromater used for the fluorescence measurements uses a grating with 600 lines per mm and is blazed at 1000 nm. The optical density for fluorescence

experiments did not exceed 0.1 OD in order to avoid inner filter effects.

Pump-probe spectroscopy. A 1 kHz regeneratively amplified Ti:Sapphire pulsed laser system (Coherent Libra, Santa Clara, CA) which generates ~45 fs pulses centered at 800 nm is directed first towards a high efficiency 50:50 beamsplitter, ultimately forming the pump and probe arms for the experiment. The reflected portion, 2.0 W of 800 nm light, is sent into a commercial optical parametric amplifier (OPerA Solo, Vilnius, Lithunia) which for our experiments, is used to generate ~60 fs pulses centered at 620 nm, 710 nm, and 950 nm, which we use as our acticinc pump. The pump pulse first traverses through a set of variable neutral density filters in order to control the incident pump power on the sample. Power dependent kinetics was observed for the QDI nanoparticle for pump powers above 15 uW, and hence all experiments undertaken were carefully controlled such that the incident power was approximately was below 15 uW. The experiments themselves were done using a commercial pump-probe setup (Ultrafast system Helios, Sarasota, FL), which for the pump arm included an optical chopper set to 500 Hz as well as a 400 mm focal length lens to focus into the sample.

The transmitted portion of the first 50:50 beamsplitter is split again with a 90:10 beamsplitter, with the reflected portion dumped using a beamblocker and the transmitted portion directed into the Helios setup. It is first physically delayed using multiple passes on the Helios's optical delay line, capable of pump-probe delays up to ~7.4 ns. Once the beam exits the delay line, it is shaped using an iris to reduce the diameter from ~6 mm to ~1.5 mm. The resultant light is directed through a λ/2 waveplate and polarizer combination to both control the polarization of the probe light as well as for attenuation prior to white light supercontinuum generation. This white light is generated by focusing the remaining 800 nm probe light into a 3 mm sapphire crystal, generating white light from 450 nm to 800 nm. The resultant probe light is refocused into the sample at the same position as the pump beam after passing through a shortpass filter to reject the remaining 800 nm fundamental. The probe light which transmits through the sample is recollimated and focused into a fiber optic connected to a detector. Difference absorption spectra (ΔA) were calculated by alternative measuring the absorption of the probe light in the "pump on" condition and the "pump off" condition according to the 500 Hz optical chopper. An integration time of 1 s per pump-probe delay was used, and scans were generally averaged for more than 100 scans without any sign of degradation. A broadband λ/2 waveplate in the pump arm was used to control the polarizations to both magic angle configuration for the experiments probing population dynamics as well as to the parallel configurations for the pump-probe anisotropy experiments. Pump probe anisotropy was calculated using the following equation:

$$Anisotropy(\lambda,t) = \frac{\Delta A_{parallel}(\lambda,t)}{2\Delta A_{magic}(\lambda,t)} - \frac{1}{2}$$

which can be trivially derived from more standard calculations of anisotropy.

Global analysis. Global analysis was undertaken using the Glotaran package software package, which is freely available and allows the user to specify a particular number of states, for which the program will then model the kinetic evolution of the transient spectra according to the number of states provided in order to minimize the residual between the global fit and the data itself.[23] We assume the photophysical dynamics will take the form of exponential decays for the processes studied, which is appropriate for unimolecular kinetics. Prior to global analysis fitting, the pump probe spectra were background subtracted and chirped corrected using the Ultrafast Systems Surface Xplorer software, which averages and subtracts the spectra prior to time zero and fits a polynomial to user selected points to compensate for group velocity dispersion in the white light, respectively. We employ a sequential model in analyzing our global analysis, meaning that the resultant spectral depiction of the extracted time constants are evolution associated decay spectra (EADS). Briefly, each EADS is a representative spectrum which decays with a particular time constant to the subsequent EADS, and so on depending on the number of states in the user designated model.

Results and Discussion

Steady-state nanoparticle characterization. Absorption spectra of the unitary and a range of binary nanoparticles with different VONc and QDI loadings are reported in Figure 2a. The composition of the binary nanoparticles is modified by adjusting the relative concentration of the individual chromophores in the precursor solution, which is reported for binary 1 through 3 in the Supplementary Information (S1). There is notable strong excitonic coupling in both QDI and VONc nanoparticle absorption spectra, showing strong blueshifts compared to the spectra of individual VONc and QDI in toluene solution (Figure 1). The blueshift is indicative of H-like aggregates in both nanoparticles, implying π-π stacking as the major form of intermolecular interaction between neighboring chromophores, which is not only reflective in the crystal structures of similar molecules, but makes sense in the context of their molecular structure as mostly flat, π-conjugated systems.[24-27]

Starting from a purely QDI nanoparticle, increasing the amount of VONc in the precursor solution shifts the absorption maximum from the QDI peak (λ_{max} = 715 nm) towards the absorption maximum of the purely VONc nanoparticle (λ_{max} = 749 nm), as well as changing the overall shape of the absorption features to that more like the VONc nanoparticle. The absorption spectra of the

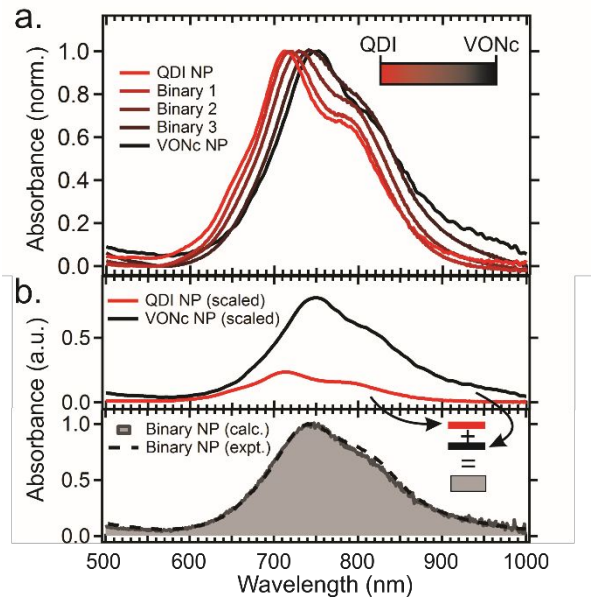

Figure 2. Absorption spectra of unitary and binary nanoparticles composed of QDI and VONc molecules, where (a) displays that the binary nanoparticles have absorption spectra which depend on the respective fraction of QDI and VONc while (b) demonstrates that the binary absorption spectra are linear combinations of scaled absorption spectra of QDI and VONc unitary nanoparticles.

binary nanoparticles studied were shown to be accurately described by linear combinations of the absorption spectra of individual QDI and VONc nanoparticle solutions, shown pictorially for Binary 3 in Figure 2b, where the calculated spectrum is prepared from the closest matching linear combination of absorption spectra by scaling the QDI and VONc nanoparticle absorption spectra and taking their sum. This was also shown with an explicite mixture of QDI and VONc nanoparticles in figure S10. The fact that the binary nanoparticle absorption spectra can be reconstituted as linear combinations of the individual QDI and VONc nanoparticles means that not only does the doping of VONc molecules into QDI nanoparticles and vice-versa not disturb the intermolecular interactions within the individual QDI nanoparticles, but that when they are in the same nanoparticle, they do not strongly interact such that new absorption features arise, such as new charge transfer state absorptions.[28] This leads us to believe that there is strong enough phase separation between the VONc and QDI domains within the binary nanoparticles that there is no disturbance of each respective domains' photophysical properties due to relatively weak QDI/VONc inter-domain coupling.

The issue that arises from the result of weak coupling between the QDI and VONc in a single nanoparticle is that this cannot be spectroscopically distinguished from a solution of unitary QDI and VONc nanoparticles with a linear absorption measurement. New photophysical interactions upon photoexcitation of either the QDI or VONc excitonic transitions within the nanoparticle would in practice change the steady-state fluorescence of the system, especially if new photoinduced charge transfer (PCT) pathways became active, where one would expect a quenching of the excited state luminescence.[29] Both the QDI and VONc nanoparticles, however, already exhibit undetectable fluorescence with our current equipment, making the fluorescence quenching experiment inconclusive (S6-9). Hence, in order to decisively test the existence of mixed composition organic nanoparticles, ultrafast time-resolved spectroscopy would be necessary to investigate whether there are any distinct photophysical dynamics in the binary nanoparticles compared to the unitary ones.

Ultrafast pump-probe spectroscopy on unitary and binary nanoparticles. A full description of the ultrafast-pump probe spectroscopy can be found in the Experimental Methods. Briefly, we use a narrowband pump pulsed excitation to excite excitons in the unitary and binary nanoparticles, while using a second white light probe pulse with fixed time delay to the pump pulse to track the spectral evolution from the femtosecond to the nanosecond time scale. The resultant spectral evolution was then fit using the Glotaran global analysis software to extract evolution associated decay spectra (EADS) from the pump probe measurements, the results for which are summarized in Table 1. Global analysis for all samples and representative kinetic traces can be found in the Supplementary Information (S12-42).

The QDI organic nanoparticle displayed a monoexponential decay to the ground state, following a presumed ultrafast excitonic relaxation from the upper singlet exciton state S_+ to the lower state S_- on a timescale faster than the time resolution of our experiment (~100 fs, dictated by the pump pulse duration).[30] The fact that this photoexcited state is a dark, lower lying excitonic state is further corroborated by the lack of fluorescence detected from a solution of these nanoparticles, despite QDI molecules simply in toluene solution displaying finite, albeit small, fluorescence intensity (S6). Furthermore, this photoexcited state decays directly to the ground state with a time constant of 220 ps, which is slightly slower than the nonradiative decay measured for QDI in solution (S11-17). Importantly, the shape of the pump-probe spectrum has a characteristic ground state bleach (GSB) with peak maximum at 710 nm with a broad, low intensity excited state absorption (ESA) spanning from 450 to 600 nm.

The VONc nanoparticle, on the other hand, displays a slightly richer set of photophysical dynamics. Photoexcitation of the VONc nanoparticle still at 620 nm first results in a GSB feature centered at 740 nm along with a broad, double peaked ESA feature with local maxima at 475 and 660 nm. Subsequently, with a time constant of 5.8 ps, there is a noticeable blueshift and change in shape of the ESA spectrum, changing from this double-peaked feature from the initial photoexcited state to a spectrum with a single maximum, located at 605 nm. It has been reported by others that in VONc films, there is an ultrafast intersystem crossing following photoexcitation with the singlet lifetime on the order of picoseconds.[31] Comparing the ESA structure of the EADS of the

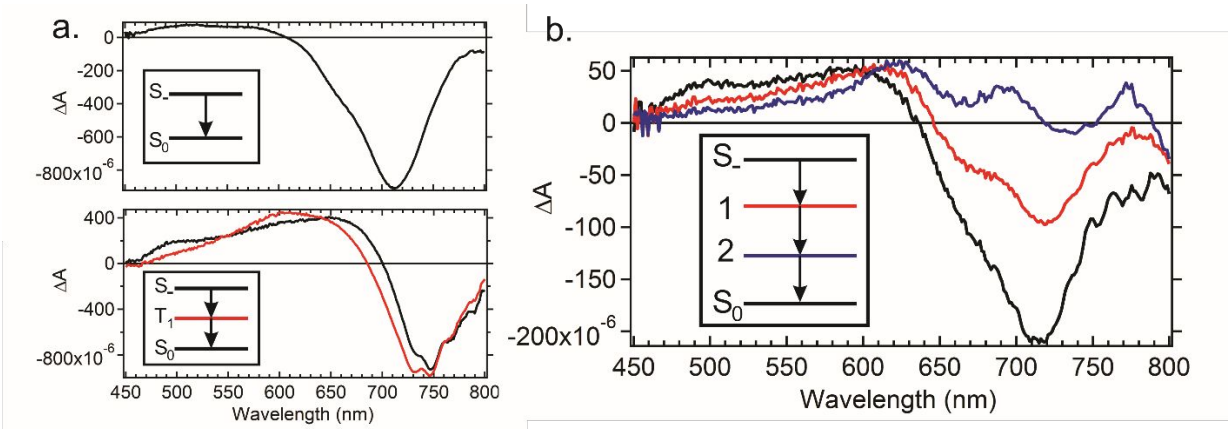

Figure 3. (a) Global analysis with sequential modeling of the pump-probe spectra following the photoexcitation at 620 nm of a solution of QDI nanoparticles (top) and VONc nanoparticles (bottom). (b) Global analysis with sequential modeling of the pump-probe spectra following the photoexcitation at 710 nm of Binary 1, which is composed mostly of QDI.

VONc nanoparticle to that of VONc in solution (S22-32) brings us to a similar conclusion—that the VONc exciton is also undergoing ISC, albeit faster than its molecular counterpart. The robustness of the intensity and position of the negative feature in the VONc nanoparticle pump probe spectrum throughout ISC also supports the assumption that there also exists some ultrafast relaxation from the higher energy, optically accessible S_+ state to a dark S_- state, and it is from this S_- state that the exciton undergoes ISC. The possibly reduced energy gap between the S_- state and the produced triplet state may partially explain the ISC speed-up between VONc in nanoparticle form from purely VONc in solution from strictly energy gap law considerations.[32]

Photoexcitation of the binary nanoparticles, particularly those with high QDI loading or with excitation more resonant with QDI optical excitation affords a familiar initial transient spectrum, but starkly distinct dynamics. This is exemplified by looking at the pump probe dynamics of Binary 1 from Figure 2, which is composed of mostly QDI, shown in Figure 3b. Using a pump wavelength of 710 nm, near resonant with the absorption maximum of QDI, we see key transient features associated with the QDI S_- exciton. This feature has a lifetime of only 6.6 ps, evolving into a completely new spectrum with slightly diminished ESA and seemingly a marked decrease in GSB. This new spectrum decays with a time constant of 70 ps into another spectrum with further decreased ESA from 450 to 600 nm, but on top of the GSB arises a second overlapping ESA feature. This new spectrum has a lifetime longer than the physical limits of the delay stage (7.4 ns), much longer than that of either individual nanoparticle as well. These new dynamics point to a new set of photophysical interactions which only occur following the photoexcitation of nanoparticles composed from a precursor solution of both QDI and VONc, pointing towards the creation of a binary nanoparticle.

Table 1. EADS Lifetimes for Nanoparticles in Figure 3.

Nanoparticle	EADS 1 (ps)	EADS 2 (ps)	EADS 3 (ps)
QDI	220	N/A	N/A
VONc	5.8	4300	N/A
Binary 1	6.6	70	>7000

We can further characterize the nature of this binary nanoparticle by first digging deeper into the results from the Global Analysis. Excitation energy transfer can be ruled out by the basis that neither of the EADS, or states 1 and 2 in Figure 3b, retain the spectra of the individual QDI or VONc nanoparticle spectra. Photoinduced triplet transfer from the VONc to the QDI is plausible, but is not consistent with the trend of a higher degree of these new transient features being formed from photoexcitation on the blue side of the absorption spectrum, which is more consistent with a QDI* photoinduced process. Further, photoinduced triplet transfer would have to occur on a timescale much shorter than ISC of the VONc exciton, since the VONc ISC spectral evolution EADS are not observed. This leaves the possibility of photoinduced charge transfer, which is the process by which an excited chromophore transfers an electron or hole to a neighboring chromophore, forming their respective cations or anions.[33]

In fact, photoinduced charge transfer to form the VONc cation, $VONc^+$, and the QDI anion, QDI^-, seems as though it would be exergonic when considering the approximated energy of the charge transfer state, 1.2 eV, taken from literature electrochemical values of the individual molecules in solution[34, 35], as well as an approximated energy of the QDI S_- state, 1.4 eV, approximated by estimating the S_- state energy to be equidistant energetically from the QDI S_1 energy in solution to the optically bright state in the QDI nanoparticle absorption spectrum, but instead shifted towards the red. Using these energetic parameters, the extracted short-time rate constant, and by assuming a dielectric environment comparable to condensed phase organic systems ($\varepsilon = 3$), we calculate the coupling to be 0.07 eV, firmly in the weak coupling regime of electron transfer. A more detailed discussion can be found in the Supplementary Information (S44). Further evidence of electron transfer comes from taking the absorption spectrum of a VONc in THF solution that has been chemically oxidized by tris(4-bromophenyl)ammoniumyl hexachloroantimonate, or magic blue. The absorption spectrum that results from the magic blue addition, shown in the Figure 4, exhibits a new absorption feature at 735 nm, which is in the same region where we see the new ESA in the last EADS of the binary nanoparticle.

Assigning this new photoinduced process to photoinduced hole transfer (PHT) still requires an explanation of EADS2, which is formed with a time constant of 0.15 ps^{-1}. We find that upon subtraction of EADS1 from EADS2 and EADS2 from EADS3,

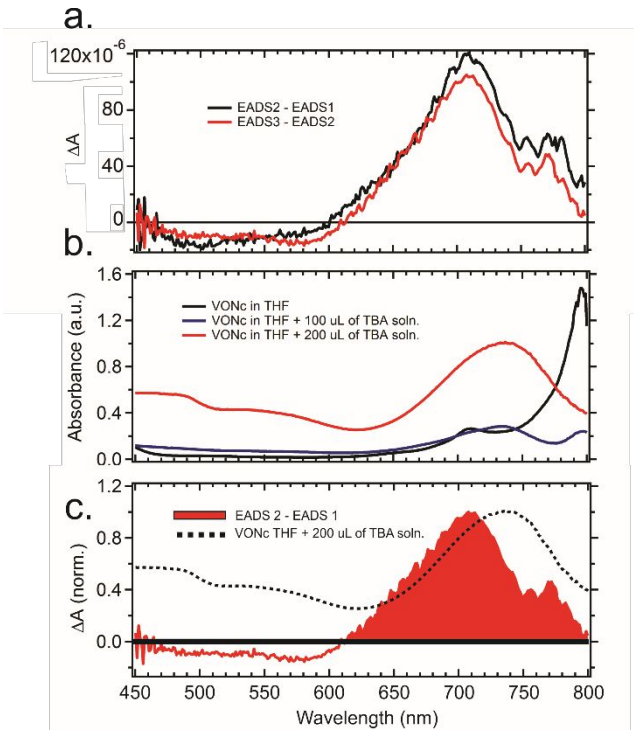

Figure 4. (a) Resultant spectra taken by subtracting EADS 1 from EADS 2 and EADS 2 from EADS 3 in the case of the Binary 1 Global analysis shown in Figure 3. (b) Absorption spectra of VONc in THF solution, as well as the same solution after the addition of a chemical oxidant, quenching its ground state absorption and giving rise to a new absorption feature in the NIR. (c) Comparison of the first difference EADS spectrum from 4a and the presumed $VONc^+$ absorption, hinting at their similar spectra.

representative spectra of which features are exactly changing in time become apparent, shown in figure 4a. These new difference spectra are remarkably similar, displaying what we interpret as an increase in a new, broad excited state absorption from 600 to 800 nm, reflecting almost exactly the $VONc^+$ absorption spectra, with slight differences due to the presumed introduction of a new VONc GSB signal which should appear as a result of photoinduced hole transfer to a VONc molecule in the ground state.

This result implies that both the 6.6 ps and the 70 ps lifetime component both correspond to PHT, which is actually a relatively common result in the realm of thin film organic blends that undergo photoinduced electron transfer, where the shorter time component corresponds to charge transfer from an exciton at the donor-acceptor interface and the longer lifetime component arises from charge transfer events which occur after the diffusion of excitons from the bulk of the donor material to the donor-acceptor interface.[36-38] With this assignment, we can now estimate the efficiency of the charge transfer of Binary 1 considering both direct and diffusion-limited charge transfer to be ~87%, the calculation procedure shown in the Supplementary Information (S45). Pump-probe anisotropy measurements of QDI unitary nanoparticles report an excitation hopping time of approximately 65 ps (S43), meaning that it is a feasible interpretation to apply this immediate/delayed charge transfer picture to our system.

Co-core dependent ultrafast pump-probe spectroscopy. In order to explore this possibility to a greater extent, we then synthesized a series of binary nanoparticles with an increasing amount of polystyrene (PS) while retaining the same QDI/VONc ratio in the organic precursor solution, in an attempt to add an innocent filler type material into the binary nanoparticles and measure the changes to the ultrafast photophysics as a result of that addition. Representative physical and photophysical properties are shown in Figure 4, where increasing (PS) loading leads to an overall increase in nanoparticle size as well as a redshift in the absorption spectra. Importantly, there is a clear change in the photophysical dynamics upon inclusion of the PS co-core, exemplified in the kinetics shown in Figure 4a, with the Global Analysis tabulated in Table 2.

On the increase of PS in the precursor solution from 0 to 10 and 20 mg/mL, we see a large increase in predominantly the second time component of the PHT. Along the lines of a diffusion limited PHT for the lifetime of the second EADS, it follows that upon the increase and assumed lengthening of the distance between the QDI and VONc domains within a singular nanoparticle, the number of excitation hopping events that are necessary prior to reaching the QDI-VONc and undergoing PHT increases, reflecting the increase in the lifetime associated with the second EADS. Further, the first EADS lifetime is relatively unaffected by this PS addition, further supporting the assignment of the first EADS decay as being that of interfacial photoexcitation and immediate charge transfer. We speculate that the increase of the first lifetime to 15 ps for the highest PS loading case reported in Table 2 could be due to a decrease in QDI or VONc intradomain interactions, resulting in slightly different interdomain coupling from a less delocalized excitonic state or augmented charge transfer energetics, and hence a slightly slower PHT. More specifically, the addition of increasing amounts PS may result in smaller QDI aggregates within the nanoparticle, such that once the aggregate sizes becomes smaller there may be less delocalization of the anion species, which would slow down charge transfer.

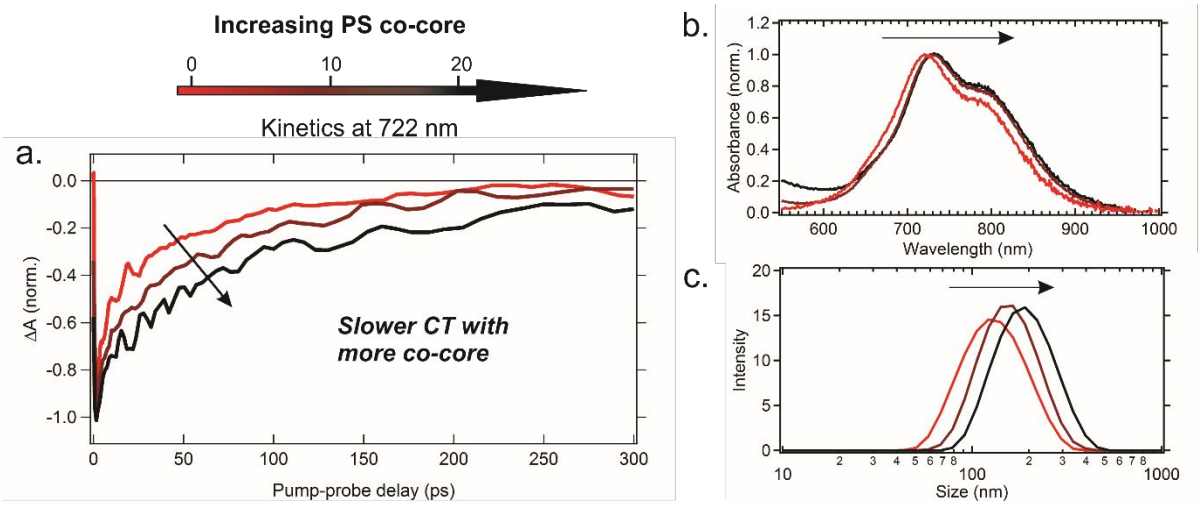

Figure 5. Changes to the photophysical properties of the binary 1 nanoparticle upon increasing addition of co-core from with 0, 10, and 20 mg/mL of polysterene (PS) added to the organic precursor solution prior to FNP. (a) Decreasing rates of charge separation are observed with an increase in PS co-core measured with pump-probe spectroscopy, for which all cases were photoexcited at 710 nm and the kinetic trace is shown for 722 nm probe wavelength. (b) Absorption spectra of the increasing co-core cases, showing an overall small redshift with increasing co-core. (c) DLS spectra recorded for increasing co-core, displaying increasing average particle size.

	Average Z diameter (nm)	PDI	EADS 1 (ps)	EADS 2 (ps)	EADS 3 (ps)
Binary 1	90.3	0.17	6.6	70	>7000
Binary 1 with 10 mg/ mL PS co-core	169.7	0.15	6.8	97	>7000
Binary 1 with 20 mg/ mL PS co-core	186.5	0.17	15	185	>7000

Table 2. Physical and Photophysical Properties of Binary Nanoparticles with Added PS Co-core.

Conclus

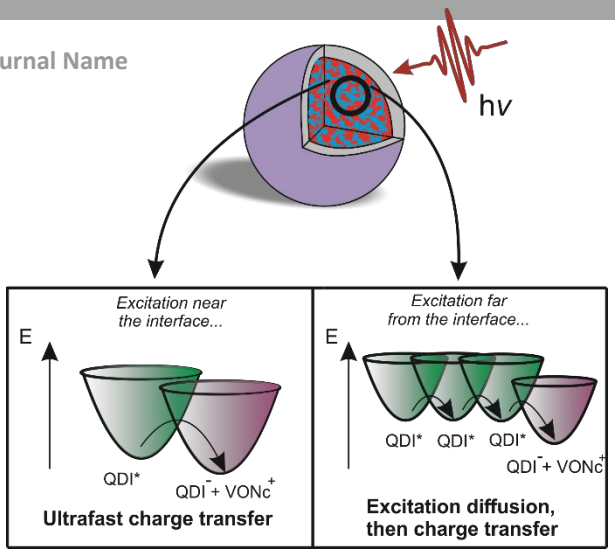

Figure 6. Diagram displaying the two components of photoinduced hole transfer after photoexcitation with NIR light, with the potential energy surfaces on the left reflecting direct photoexcitation at the interface and inmmediate ultrafast charge transfer, while the right displays an example of charge transfer after QDI excitation diffusion to the QDI/VONc interface.

ions

In conclusion, we have reported the preparation of binary nanoparticles from to form binary nanoparticles from small organic molecules using Flash Nanoprecipitation. This synthetic technique may prove to be general in its ability to form mixed composition nanoparticles without necessitating that composition to include polymeric substituents. The possibility of bringing organic blend photophysics like charge transfer, energy transfer, and triplet sensitization to the nanoscale allows for the design of new tailored functional organic nanoparticles. The nanoparticles reported herein have broad, strong absorption in the NIR, meaning that their use as photoacoustic imaging or photoablative therapy agents is not only possible, but may bring to light new design principles for these biotechnologies. From the photophysical perspective, we demonstrated that these organic blends on the nanoscale exhibit a similar set of photophysical interactions as those of macroscopic organic blends that are currently used in the highest efficiency OPVs, exhibiting not only ultrafast charge transfer from photoexcitation at the interface, but also an exciton migration step that occurs from photoexcitations further from the interface which also can generate photocurrent, summarized pictorially in Figure 6.[39, 40] The relatively long lifetime of the charge carriers in this binary nanoparticle further may point to efficient charge migration away from the QDI/VONc interface, and may be useful as a model system to avoid geminate recombination in OPV active layers, although longer pump-probe delays will be necessary to pinpoint the exact recombination kinetics.[41] Overall, these results serve to break open the field of organic nanoparticles, displaying that not only are organic mixtures of small molecules possible on the nanoscale, but that they can have photophysical properties akin to their macroscale blends.

Conflicts of interest

There are no conflicts to declare.

Acknowledgements

This material is based on work supported by the National Science Foundation Graduate Research Fellowship under Grant Number DGE-1656466 (to B.K.). G.D.S. gratefully acknowledges the Division of Chemical Sciences, Geosciences, and Biosciences, Office of Basic Energy Sciences of the U.S. Department of Energy through Grant No. DE-SC0015429. We are grateful for support from the Princeton University Center for Health and Wellbeing (HDL), Woodrow Wilson School of Public and International Affairs Program in Science, Technology, and Environmental Policy (HDL). This work was supported by the Princeton University SEAS grant from the Old School Fund (RKP).

Notes and references

1 T. Kietzke, D. Neher, K. Landfester, R. Montenegro, R. Guntner and U. Scherf, *Nat Mater*, 2003, **2**, 408-412.
2 S. Sankaran, K. Glaser, S. Gärtner, T. Rödlmeier, K. Sudau, G. Hernandez-Sosa and A. Colsmann, *Organic Electronics*, 2016, **28**, 118-122.
3 M. Bag, T. S. Gehan, L. A. Renna, D. D. Algaier, P. M. Lahti and D. Venkataraman, *RSC Adv.*, 2014, **4**, 45325-45331.
4 L. A. Renna, C. J. Boyle, T. S. Gehan and D. Venkataraman, *Macromolecules*, 2015, **48**, 6353-6368.
5 K. K. Ng and G. Zheng, *Chem Rev*, 2015, **115**, 11012-11042.
6 R. D. Pensack, A. J. Tilley, S. R. Parkin, T. S. Lee, M. M. Payne, D. Gao, A. A. Jahnke, D. G. Oblinsky, P. F. Li, J. E. Anthony, D. S. Seferos and G. D. Scholes, *J Am Chem Soc*, 2015, **137**, 6790-6803.
7 T. Asahi, T. Sugiyama and H. Masuhara, *Acc Chem Res*, 2008, **41**, 1790-1798.
8 S. N. Clafton, D. M. Huang, W. R. Massey and T. W. Kee, *J Phys Chem B*, 2013, **117**, 4626-4633.
9 Z.-m. Ou, H. Yao and K. Kimura, *Journal of Photochemistry and Photobiology A: Chemistry*, 2007, **189**, 7-14.
10 H. Nakanishi and H. Oikawa, 2003, DOI: 10.1007/978-3-642-55545-9_2, 17-31.
11 R. Kabe and C. Adachi, *Nature*, 2017, **550**, 384-387.
12 Y. L. Lin, M. Koch, A. N. Brigeman, D. M. E. Freeman, L. Zhao, H. Bronstein, N. C. Giebink, G. D. Scholes and B. P. Rand, *Energy Environ. Sci.*, 2017, **10**, 1465-1475.
13 K. N. Schwarz, S. B. Farley, T. A. Smith and K. P. Ghiggino, *Nanoscale*, 2015, **7**, 19899-19904.
14 H. Yao and K. Ashiba, *Chemphyschem*, 2012, **13**, 2703-2710.
15 X. Wang, L. Liu, S. Zhu, J. Peng and L. Li, *RSC Advances*, 2017, **7**, 40842-40848.

16 O. Salata, *J Nanobiotechnology*, 2004, **2**, 3.
17 H. D. Lu, T. L. Lim, S. Javitt, A. Heinmiller and R. K. Prud'homme, *ACS Comb Sci*, 2017, **19**, 397-406.
18 H. D. Lu, B. K. Wilson, T. L. Lim, A. Heinmiller and R. K. Prud'homme, *ACS Biomaterials Science & Engineering*, 2017, **3**, 443-451.
19 F. X. Gu, R. Karnik, A. Z. Wang, F. Alexis, E. Levy-Nissenbaum, S. Hong, R. S. Langer and O. C. Farokhzad, *Nano Today*, 2007, **2**, 14-21.
20 B. K. Johnson and R. K. Prud'homme, *Australian Journal of Chemistry*, 2003, **56**, 1021.
21 M. Akbulut, P. Ginart, M. E. Gindy, C. Theriault, K. H. Chin, W. Soboyejo and R. K. Prud'homme, *Advanced Functional Materials*, 2009, **19**, 718-725.
22 H. D. Lu, L. Z. Wang, B. K. Wilson, S. A. McManus, J. Jumai'an, P. K. Padakanti, A. Alavi, R. H. Mach and R. K. Prud'homme, *ACS Appl Mater Interfaces*, 2018, DOI: 10.1021/acsami.7b07242.
23 J. J. Snellenburg, S. P. Laptenok, R. Seger, K. M. Mullen and I. H. M. v. Stokkum, *Journal of Statistical Software*, 2012, **49**.
24 F. C. Spano, *Acc Chem Res*, 2010, **43**, 429-439.
25 M. Kasha, *Radiation Research*, 1963, **20**, 55.
26 H. Wang, Y. Zhou, V. A. L. Roy, D. Yan, J. Zhang and C.-S. Lee, *Organic Electronics*, 2014, **15**, 1586-1591.
27 F. Nolde, W. Pisula, S. Müller, C. Kohl and K. Müllen, *Chemistry of Materials*, 2006, **18**, 3715-3725.
28 F. E. Osterloh, M. A. Holmes, J. Zhao, L. Chang, S. Kawula, J. D. Roehling and A. J. Moulé, *The Journal of Physical Chemistry C*, 2014, **118**, 14723-14731.
29 D. Rehm and A. Weller, *Israel Journal of Chemistry*, 1970, **8**, 259-271.
30 J. C. Dean, D. G. Oblinsky, S. Rafiq and G. D. Scholes, *J Phys Chem B*, 2016, **120**, 440-454.
31 F. Ito, T. Inoue, D. Tomita and T. Nagamura, *J Phys Chem B*, 2009, **113**, 5458-5463.
32 R. Englman and J. Jortner, *Molecular Physics*, 1970, **18**, 145-164.
33 M. R. Wasielewski, *Chemical Reviews*, 1992, **92**, 435-461.
34 S. K. Lee, Y. Zu, A. Herrmann, Y. Geerts, K. Müllen and A. J. Bard, *Journal of the American Chemical Society*, 1999, **121**, 3513-3520.
35 N. Kobayashi, S. Nakajima, H. Ogata and T. Fukuda, *Chemistry*, 2004, **10**, 6294-6312.
36 M. Pope and C. Swenburg, *Electronic Processes in Organic Crystals Polymers*, Oxford University Press, New York, 1999.
37 A. J. Heeger, *Adv Mater*, 2014, **26**, 10-27.
38 A. Haugeneder, M. Neges, C. Kallinger, W. Spirkl, U. Lemmer, J. Feldmann, U. Scherf, E. Harth, A. Gügel and K. Müllen, *Physical Review B*, 1999, **59**, 15346-15351.
39 B. Kippelen and J.-L. Brédas, *Energy & Environmental Science*, 2009, **2**, 251.
40 S. M. Menke, W. A. Luhman and R. J. Holmes, *Nat Mater*, 2013, **12**, 152-157.
41 D. Credgington, F. C. Jamieson, B. Walker, T. Q. Nguyen and J. R. Durrant, *Adv Mater*, 2012, **24**, 2135-2141.